Meas. Sci. Technol. **19** (2008) 085202 (11pp) doi:10.1088/0957-0233/19/8/085202

Methods for in-field user calibration of an inertial measurement unit without external equipment

W T Fong, S K Ong and A Y C Nee

Mechanical Engineering Department, Faculty of Engineering, National University of Singapore, 9 Engineering Drive 1, Singapore 117576

E-mail: wtfong@nus.edu.sg, mpeongsk@nus.edu.sg and mpeneeyc@nus.edu.sg

Received 14 November 2007, in final form 14 May 2008
Published 10 July 2008
Online at stacks.iop.org/MST/19/085202

Abstract

This paper presents methods to calibrate and compensate for non-zero biases, non-unit scale factors, axis misalignments and cross-axis sensitivities of both the tri-axial accelerometer and gyroscopic setups in a micro-electro-mechanical systems (MEMS) based inertial measurement unit (IMU). These methods depend on the Earth's gravity as a stable physical calibration standard. Specifically, the calibration of gyroscopes is significantly improved by comparing the outputs of the accelerometer and the IMU orientation integration algorithm, after arbitrary motions. The derived property and proposed cost function allow the gyroscopes to be calibrated without external equipment, such as a turntable, or requiring precise maneuvers. Both factors allow the IMU to be easily calibrated by the user in the field so that it can function as an accurate orientation sensor. A custom-made prototype IMU is used to demonstrate the effectiveness of the proposed methods, with data that are carefully obtained using prescribed motions, as well as those less rigorously collected from the IMU when it is mounted on the head of a user or held in hands with brief random movements. With calibration, the observed average static angular error is less than a quarter of a degree and the dynamic angular error is reduced by a factor of 2 to 5.

Keywords: calibration, inertial, gyroscopes, accelerometers, error compensation and model fitting

1. Introduction

An inertial measurement unit (IMU) generally consists of orthogonally mounted accelerometers and gyroscopes to measure the accelerations and angular velocities, respectively. Micro-electro-mechanical systems (MEMS) technologies have enabled miniature sensors suitable for human scale inertial sensing in fields such as augmented reality (AR) tracking and biomechanical measurements, where the accelerations, angular velocities and orientations of the head, limbs and back of a human subject can be measured. These low-cost sensors can be easily incorporated into custom-built IMUs, but do not function well as inertial trackers without calibration, which removes the systematic sensor errors. For AR, these errors can result in discernable gaps that will mar the illusion that a virtual object has been augmented onto a real world object. Although calibrated IMUs are commercially available, it may be attractive to build IMUs to achieve smaller sizes and better ergonomics, to take timely advantage of newer, higher performance sensors, to circumvent the limitations of commercial units or reduce costs. Outside the inertial navigation field, calibration can be challenging due to the lack of certified calibration equipment. The purpose of this work is to demonstrate simple and yet effective accelerometer and gyroscope calibration methods to improve the accuracy of the orientation measured using a custom-built IMU. As an independent three degrees of freedom (3DOF) tracker, the custom-built IMU calibrated using the methods proposed in this paper is capable of measuring the orientation with respect to the Earth's gravity vector with an average static angular error of 0.23°. This IMU can also be combined with position sensors to form hybrid, six degrees of freedom (6DOF) trackers, which

can measure both position and orientation. Examples of hybrid 6DOF trackers with IMUs are presented by Titterton and Weston (1997), Foxlin and Naimark (2003), Niu and El-Sheimy (2005), Semeniuk and Noureldin (2006), as well as El-Gizawy *et al* (2006).

For low-cost MEMS sensors, it is not economical to procure expensive equipment that costs many times more than the cost of the sensors to quantify the errors of these sensors so that they can meet the requirements of human scale inertial measurement. This forms the motivation to find calibration methods that do not rely on high physical precision to fully exploit the available accuracy of current MEMS sensors. As an illustration, the maximum zero bias and sensitivity of a MEMS accelerometer at the time of writing this paper are 0.1 g and 0.001 g, respectively. One way to directly measure the zero bias of an accelerometer is to mount it with its axis perpendicular to the Earth's gravity vector, such that a zero reading can be expected. In such a position, the accelerometer can detect derivations as small as $\sin^{-1}(0.001) = 0.06^\circ$ from the gravity vector. Therefore, in order to fully exploit the sensitivity of the accelerometer so as to accurately determine the zero bias, the combined tolerance of the test equipment and the mounting should be tighter than 0.01° with respect to the gravity vector.

The Earth's gravity is used as the physical standard for calibrating the IMU; it is readily available and is a very stable quantity. A tri-axial accelerometer is calibrated using property (**p1**): *the magnitude of the static acceleration measured must equal that of the gravity* (Lötters *et al* 1998). This is a tri-axial orthogonal constraint, where values measured on each axis are not independent. For a tri-axial gyroscopic system, property (**p2**) is proposed here: *the gravity vector measured using a static tri-axial accelerometer must equal the gravity vector computed using the IMU orientation integration algorithm, which in turn uses the angular velocities measured using the gyroscopes.* This property holds whenever the IMU is static after arbitrary motions. Both properties (**p1**) and (**p2**) impose physical and mathematical constraints on the sensor outputs, which are used to calibrate the sensor errors instead of relying on high physical precision. As precise motions and externally generated calibration standards are not required, the IMU can be easily calibrated by the users in the field. It is possible to calibrate the IMU by holding it in the hands and moving it for a few minutes, as shown in the latter part of this paper. This greatly reduces the time and difficulties involved in calibrating the IMU, especially for the gyroscope.

The sensor errors considered are the non-zero bias, non-unit scale factor, non-orthogonal misalignment of the sensor axes and the cross-axis sensitivity. The calibration process proceeds by first defining the sensor error models, deriving the two cost functions using (**p1**) and (**p2**) respectively, collecting the raw measurements and fitting the model parameters based on nonlinear optimization of the cost functions.

2. Previous works

High-end inertial sensor calibration and error modeling are well-established fields (Titterton and Weston 1997). The basic idea is to compare the sensor output with known values generated using calibration instruments. Researchers have also used optical trackers (Kim and Golnaraghi 2004) and the Kalman filter with precise maneuvers (Grewal *et al* 1991, Foxlin and Naimark 2003) to calibrate low-end inertial sensors for less demanding applications. In previous methods, the main difficulties are in the generation of accurate external calibration values, as well as precisely mounting and moving the IMU. These often require costly specialized equipment and high-precision equipment which may not be available to researchers who are seeking to use the IMU for orientation measurements. A recent development in biomechanical tracking (Lötters *et al* 1998) proposed the use of (**p1**) to calibrate accelerometer biases and scale factors. Their method does not require precise inclinations and model parameters are fitted using robust estimation techniques. This was extended by Skog and Händel (2006) to include sensor axis misalignment, their tri-axial accelerometer error model which converts the kth acceleration vector measured in the sensor frame, $\boldsymbol{a}_{S,k}$, to the platform frame, $\boldsymbol{a}_{P,k}$, is

$$\boldsymbol{a}_{P,k} = \mathbf{MS}(\boldsymbol{a}_{S,k} - \boldsymbol{b}_a), \tag{1}$$

where the bias vector is $\boldsymbol{b}_a$, the misalignment matrix

$$\mathbf{M} = \begin{pmatrix} 1 & -\alpha_{yz} & \alpha_{zy} \\ 0 & 1 & -\alpha_{zx} \\ 0 & 0 & 1 \end{pmatrix},$$

and the scale matrix

$$\mathbf{S} = \begin{pmatrix} s_{xx} & 0 & 0 \\ 0 & s_{yy} & 0 \\ 0 & 0 & s_{zz} \end{pmatrix}.$$

α_{ij} is the small rotation of the sensor ith axis about the platform jth axis, to align with the platform ith axis. Skog and Händel (2006) proposed a similar model for calibrating the gyroscopes, but the derived cost function would require a turntable with turn rates accurate to within 0.1° per second for an MEMS-based gyroscope. Therefore, their gyroscope calibration method is not independent of external equipment, as in the case for the accelerometer. A recent work on IMU and global positioning system integration by Syed *et al* (2007) applied an error model of a similar form and utilized 26 positions to calibrate the tri-axial accelerometer. The rotation of the Earth and a turntable are used to calibrate the gyroscope. This paper proposed the application of (**p2**) to eliminate the use of turntables, or any other specialized equipment for calibrating the gyroscope.

3. Proposed sensor error models

3.1. Tri-axial accelerometer

In this paper, the model in equation (1) is improved by considering the cross-axis sensitivities, which can be up to 5% of the full measurement scale in practical MEMS accelerometers (Analog 2006, Titterton and Weston 1997). **S** is modified as

$$\mathbf{S}^* = \begin{pmatrix} s_{xx} & s_{xy} & s_{xz} \\ s_{yx} & s_{yy} & s_{yz} \\ s_{zx} & s_{zy} & s_{zz} \end{pmatrix},$$

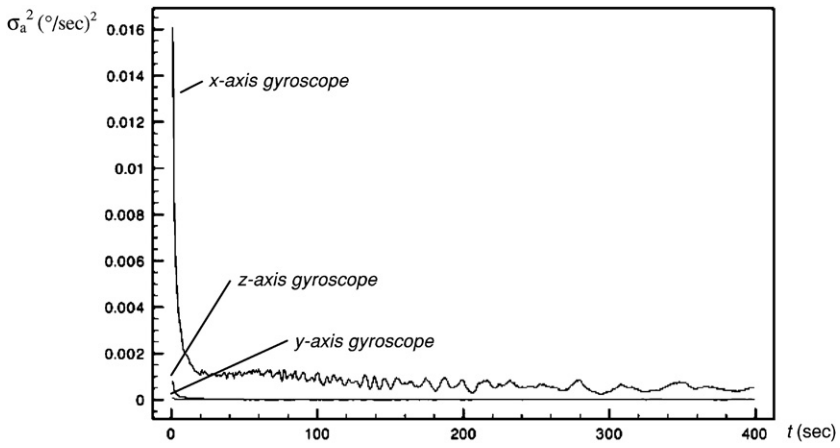

Figure 1. The Allan variance plot of the three gyroscopes in the prototype IMU.

where s_{ij} is the sensitivity of the ith axis accelerometer to the accelerations in the jth axis. Ideally, $\mathbf{S}^*$ is an identity matrix, meaning that there is no scaling errors along the axis and the sensor is not sensitive to cross-axis acceleration. As the effects of the minor cross-axis sensitivity and the sensor misalignment are similar, and there is no requirement to separate them, $\mathbf{M}$ is multiplied with $\mathbf{S}^*$ to give the matrix

$$\mathbf{E} = \begin{pmatrix} s_{xx} - s_{yx}\alpha_{yz} + s_{zx}\alpha_{zy} & s_{xy} - s_{yy}\alpha_{yz} + s_{zy}\alpha_{zy} & s_{xz} + s_{yz}\alpha_{yz} + s_{zz}\alpha_{zy} \\ s_{yx} - s_{zx}\alpha_{zx} & s_{yy} - s_{zy}\alpha_{zx} & s_{yz} - s_{zz}\alpha_{zx} \\ s_{zx} & s_{zy} & s_{zz} \end{pmatrix}$$

Ignoring the products between the off-diagonal terms of both $\mathbf{M}$ and $\mathbf{S}^*$, which have small values,

$$\mathbf{E} \approx \begin{pmatrix} s_{xx} & s_{xy} - s_{yy}\alpha_{yz} & s_{xz} + s_{zz}\alpha_{zy} \\ s_{yx} & s_{yy} & s_{yz} - s_{zz}\alpha_{zx} \\ s_{zx} & s_{zy} & s_{zz} \end{pmatrix} = \begin{pmatrix} e_{00} & e_{01} & e_{02} \\ e_{10} & e_{11} & e_{12} \\ e_{20} & e_{21} & e_{22} \end{pmatrix}.$$

$\mathbf{E}$ is a diagonally dominant correction matrix. The proposed error model for a tri-axial accelerometer setup is given in equation (2):

$$\boldsymbol{a}_{P,k} = \mathbf{E}(\boldsymbol{a}_{S,k} - \boldsymbol{b}_a). \tag{2}$$

The model parameters in matrix $\mathbf{E}$ and vector $\boldsymbol{b}_a$ are collected to form $\boldsymbol{\theta}_a = \{e_{00}, e_{01}, e_{02}, e_{10}, e_{11}, e_{12}, e_{20}, e_{21}, e_{22}, b_x, b_y, b_z,\}$ to define the function

$$h(\boldsymbol{a}_{S,k}, \boldsymbol{\theta}_a) = \mathbf{E}(\boldsymbol{a}_{S,k} - \boldsymbol{b}_a) = \boldsymbol{a}_{P,k}. \tag{3}$$

Assuming that the magnitude of gravity is unity, the cost function, similar to that proposed by Skog and Händel (2006), that measures the amount of deviation from the ideal 1 g (**p1**) for K sets of measurements is

$$\boldsymbol{L}(\theta_a) = \sum_{k=0}^{K-1} (1 - \|h(\boldsymbol{a}_{S,k}, \boldsymbol{\theta}_a)\|^2)^2. \tag{4}$$

3.2. Tri-axial gyroscopic system

The most significant source of error for gyroscopic systems is the random bias drift. The bias can be trivially measured by averaging the static gyroscope signals. However, the gyroscope biases can drift randomly over time and cause the computed orientation to be inaccurate. Practical MEMS-based IMUs use absolute orientation sensors, such as inclinometers (accelerometer) and magnetometers, to correct the drifts. However, as inclinometers and magnetometers are accurate only when the IMU is static and when the magnetic field is stable respectively, gyroscopes are still required for highly dynamic conditions. Random gyroscope bias drifts can be characterized using the Allan variance, σ_a^2 (Niu and El-Sheimy 2005, Sabatini 2006, El-Diasty *et al* 2007), which measures the variance of the difference between consecutive interval averages. It was originally used to study clock drifts and is defined as

$$\sigma_a^2 = \frac{1}{2}\sum_{k=1}^{K} (y(t,k) - y(t,k-1))^2, \tag{5}$$

where $y(t, k)$ is the kth interval average, which spans t s. Here, static gyroscope signals were collected for 1 h and analyzed by varying t from 1 s ($K = 3600$) to 400 s ($K = 9$). As t increases, the effects of noise are reduced; the value of σ_a^2 decreases and converges to the average of the random drifts. The value of least $K = 9$ is chosen so that the number of samples or interval averages is not too small for statistical reasoning to be applied. Figure 1 shows the Allan variance plot of the three gyroscopes of the prototype IMU described in section 5. The drift characteristic of the x-axis of the gyroscope is the worst as σ_a^2 takes the longest time interval of 20 s to converge, which means that the bias drift of this gyroscope is much noisier. This may be due to defects which may have occurred during the manufacturing of this gyroscope or the assembly of the IMU. This implies that the gyroscope bias should be averaged over a period of at least 20 s so that the average bias will not change significantly in the next few 20 s intervals. For the purpose of calibration, averaging the static gyroscope signals over a period of time determined using the Allan variance analysis above, will keep the bias drift minimal

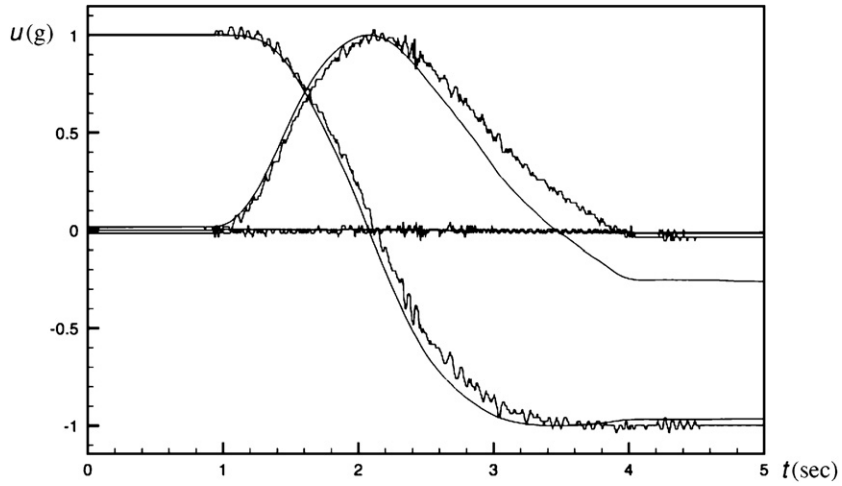

Figure 2. Plots of the three axes of u_a (jagged lines) and u_g (smooth lines) in an uncalibrated IMU.

during the following time period when the calibration data are collected.

The misalignments, scale factors and cross-axis sensitivities are modeled next. For brevity, the general notation of the accelerometer model is used, except for the turn rate vector $\boldsymbol{w} = (w_x, w_y, w_z)^{\mathrm{T}}$, in radians per second

$$\boldsymbol{w}_{P,k} = \mathbf{M}_g \mathbf{S}_g^* (\boldsymbol{w}_{S,k}), \tag{6}$$

where

$$\mathbf{S}_g^* = \begin{pmatrix} s_{xx} & s_{xy} & s_{xz} \\ s_{yx} & s_{yy} & s_{yz} \\ s_{zx} & s_{zy} & s_{zz} \end{pmatrix} \text{ and } \mathbf{M}_g = \begin{pmatrix} 1 & -\alpha_{yz} & \alpha_{zy} \\ \alpha_{xz} & 1 & -\alpha_{zx} \\ -\alpha_{xy} & \alpha_{yx} & 1 \end{pmatrix}.$$

In this model, $\boldsymbol{w}_{S,k}$ is assumed to have zero biases, i.e., the existing biases have been removed using a separate gyroscope bias model. This is because gyroscope biases change over time, while the other model parameters remain relatively constant. Therefore, the gyroscope biases have to be modeled separately. For the short duration of the calibration, the random gyroscope biases are effectively removed by averaging the static signals over 20 s. An example of a more sophisticated bias compensation technique has been reported by Sabatini (2006). $\mathbf{M}_g$ is the full misalignment correction matrix, where there is no predefined alignment, unlike for $\mathbf{M}$ (Skog and Händel 2006). As with the accelerometers, minor misalignments and cross-axis sensitivities are not distinguished and equation (6) becomes

$$\boldsymbol{w}_{P,k} = \mathbf{E}_g (\boldsymbol{w}_{S,k}). \tag{7}$$

A new cost function is proposed here using (**p2**). First, define Ψ as the operator that converts a sequence of $\boldsymbol{w}_{P,k}$, from $k = 0$ to $k = n$, and the initial gravity vector $\boldsymbol{u}_0$, to the gyroscope computed gravity vector $\boldsymbol{u}_g$. Therefore,

$$\boldsymbol{u}_g = \Psi[\boldsymbol{w}_{P,k}, \boldsymbol{u}_0] \tag{8}$$

Ψ can be any orientation integration algorithm that computes the orientation through integrating the angular velocities $\boldsymbol{w}_{P,k}$ (Titterton and Weston 1997, Savage 1998, Jekeli 2000). Here, orientation is represented using a quaternion, $\boldsymbol{q}$, and the second-order numerical integration algorithm (in section 4.2.3.1.1 of Jekeli (2000)) is used. At each time step k, the current quaternion $\boldsymbol{q}_k$ is related to the quaternion, $\boldsymbol{q}_{k-1}$, of the previous time step $k-1$ using equation (9):

$$\boldsymbol{q}_k = \left[\cos\left(0.5\,|\delta\boldsymbol{\beta}|\,\mathbf{I} + \frac{1}{|\delta\boldsymbol{\beta}|}\sin(0.5\,|\delta\boldsymbol{\beta}|)\mathbf{B}\right)\right]\boldsymbol{q}_{k-1}, \tag{9}$$

where $\delta\boldsymbol{\beta} = \boldsymbol{w}_{P,k}\,\Delta t = \begin{pmatrix} \delta\beta_x \\ \delta\beta_y \\ \delta\beta_z \end{pmatrix}$, $|\delta\boldsymbol{\beta}| = \sqrt{\delta\beta_x^2 + \delta\beta_y^2 + \delta\beta_z^2}$

and

$$\mathbf{B} = \begin{pmatrix} 0 & \delta\beta_x & \delta\beta_y & \delta\beta_z \\ -\delta\beta_x & 0 & \delta\beta_z & -\delta\beta_y \\ -\delta\beta_y & -\delta\beta_z & 0 & \delta\beta_x \\ -\delta\beta_z & \delta\beta_y & -\delta\beta_x & 0 \end{pmatrix}.$$

Δt is the time interval between the time steps and $\mathbf{I}$ is a 4×4 identity matrix. From the angular velocity, $\boldsymbol{w}_{P,k}$, measured by the gyroscopes, $\delta\boldsymbol{\beta}$ is obtained and used in equation (9) to compute the current quaternion $\boldsymbol{q}_k$ from the previous quaternion $\boldsymbol{q}_{k-1}$. Using the initial quaternion $\boldsymbol{q}_0$ and the sequence of $\boldsymbol{w}_{P,k}$ from $k = 0$ to $k = n$, the quaternion $\boldsymbol{q}_n = (a, b, c, d)^{\mathrm{T}}$ at time step $k = n$ can be obtained. The rotation matrix is obtained from $\boldsymbol{q}_n$ using equation (10):

$$\mathbf{R} = \begin{pmatrix} a^2 + b^2 - c^2 - d^2 & 2(bc + ad) & 2(bd - ac) \\ 2(bc - ad) & a^2 - b^2 + c^2 - d^2 & 2(cd + ad) \\ 2(bd + ac) & 2(cd - ab) & a^2 - b^2 - c^2 + d^2 \end{pmatrix}. \tag{10}$$

The computed gravity vector, $\boldsymbol{u}_g$, is obtained from the starting gravity vector $\boldsymbol{u}_0$, using equation (11):

$$\boldsymbol{u}_a = \mathbf{R}u_0. \tag{11}$$

Let $\boldsymbol{u}_a$ be the gravity vector measured using the static accelerometer. Figure 2 shows the divergence of $\boldsymbol{u}_a$ and $\boldsymbol{u}_g$ in an uncalibrated IMU. The jagged lines are the values of each of the three axes of $\boldsymbol{u}_a$, while the smooth lines are the corresponding values for $\boldsymbol{u}_g$, as the IMU is rotated 180° about a single axis. From figure 2, it is clear that the gyroscope sensor errors have accumulated and caused the divergence between the jagged and smooth lines to increase as the rotation continued.

The nine elements of $\mathbf{E}_g$ are collected to form $\boldsymbol{\theta}_g$, for the definition of the proposed cost function in equation (12):

$$\boldsymbol{L}(\boldsymbol{\theta}_g) = \sum_{k=0}^{K-1} \|\boldsymbol{u}_a - \boldsymbol{u}_g\|^2. \tag{12}$$

In the absence of the sensor errors and the algorithmic errors in Ψ, $\boldsymbol{u}_g - \boldsymbol{u}_a = \mathbf{0}$, whenever the IMU is static. This is true for all arbitrary motions between the static states, enabling the gyroscopes to be calibrated without accurate reference turn rates or precise maneuvers and mountings. This is an improvement over previous calibration methods presented in section 2, as the calibration process of the gyroscopes is now totally independent of external calibration values. The calibrated accelerometers, which already exist in the IMU, provide the required gravity vector measurements. This means that the IMU can be fully calibrated as it is, without any need for precision mounting on another instrument.

4. Proposed calibration procedures

This section is divided into three subsections. The first two subsections present the proposed controlled data collection procedures for both the accelerometers and the gyroscopes, which have been designed to increase the probability that the nonlinear optimization process will arrive at the correct parameter values. It is important to provide more data points than the number of parameter values to be fitted and with maximum data variability, so as to avoid pathological conditions in the function space of the cost functions. Nonlinear optimization is well known to be difficult to analyze. The numbers of data points proposed in latter sections are those that have been found to work well in simulations conducted in this study and with real data. The third subsection presents a proposed data collection procedure that is less rigorous, in which the users alternate between moving and keeping the IMU stationary. Here, only one data set is required to calibrate both the accelerometers and the gyroscopes. The variability of the data is measured statistically to ensure that the change in the orientation of the IMU is large enough to overcome the effects of the sensor noise. In the experiments, an angular difference of 10° between the static states has been found to be a good minimal value for the nonlinear optimization to produce results with the standard deviations reported in section 5.3. The resultant minimum value of the cost function is the residue error and is a measure of the fit between the sensor model and the data. A low value means that the model fits well to the data and indicates that the noise in the collected data is low as well.

In both the controlled and the less rigorous data collection calibration processes, the quasi-static detector (Saxena *et al* 2005) is used to ensure that the IMU is not subjected to motion that is humanly imperceptible but still causes significant error. As a modification to the detector proposed by Saxena *et al* (2005), only the accelerometers are required to determine the quasi-static state of the IMU. The output of each axis of the accelerometer is first high-pass filtered, followed by a rectification and then low-pass filtered. Let $\boldsymbol{a}$ be the vector of the output of a tri-axial accelerometer, *HPF*() be the high pass filter, *RECT*() be the rectification operator and *LPF*() be the low pass filter, the quasi-static state vector $\boldsymbol{s}$ is given by equation (13):

$$\boldsymbol{s} = LPF(RECT(HPF(\boldsymbol{a}))). \tag{13}$$

The square of the magnitude of the vector $\boldsymbol{s}$ can be used to detect motions and vibrations that are imperceptible to the human eye. The gyroscopes are found to be redundant as the tri-axial accelerometer can detect the angular motion as well as the linear acceleration. When the IMU is rotated, the direction of the gravity vector with respect to the IMU changes, and causes the output of each axis of the accelerometer to change. This leads the square of the magnitude of $\boldsymbol{s}$ to increase above a preset detection threshold. This greatly improves the accuracy of the static gravity vector measurements, which are required for both the accelerometer and gyroscope calibrations. The quasi-static detector is also essential when the data collection is performed in the field, where it is almost impossible to control the disturbances on the IMU.

4.1. Controlled collection of accelerometer calibration data (procedure 1)

For the tri-axial accelerometer, the IMU is placed in 18 positions, i.e., $K = 18$, to obtain 18 readings to compute the cost function $\boldsymbol{L}(\boldsymbol{\theta}_a)$. These 18 positions consist of resting the IMU on its six flat faces and 12 edges. This proposed arrangement allows gravity vector measurements to be spread evenly over the unit sphere about the center of the platform frame (Lötters *et al* 1998). As there are 12 model parameters to fit, it is prudent to have more than that number of measurements. Next, the static signals are averaged over a period of 1 s to reduce noise. $\boldsymbol{L}(\boldsymbol{\theta}_a)$ is minimized using the Downhill simplex optimization method (Press *et al* 1992). The initial parameter values are set using the nominal values. This procedure is hereafter referred to as procedure 1.

4.2. Controlled collection of gyroscope calibration data (procedure 2)

After the accelerometer has been calibrated, it can be used to serve as a static gravity vector sensor for calibrating the gyroscopes. Eighteen sets of continuous accelerometer and gyroscope samples are taken. Each set consists of 20 s of quasi-static samples for measuring the gyroscope biases and gravity vector, followed by a rotation to a new orientation and a further 1 s of quasi-static samples to measure the gravity vector in the new orientation. A period of 20 s has been determined using the Allan variance analysis in section 3.2. The IMU is mounted on a hinged surface to ease rotations. The precision of the mounting is not critical; however the mounting must be secured. Any rotation speed is acceptable as long as it spans and stays within the measurement range of the gyroscope, e.g., 300° s^{-1} for the IMU used in this paper. The main requirement is that the IMU must be rotated through large angles, so that the minute systematic errors are accumulated by the integration of the angular velocities to cause the observed divergence between $\boldsymbol{u}_g$ and $\boldsymbol{u}_a$. From equation (6), the effects of the various model parameters can only be observed when

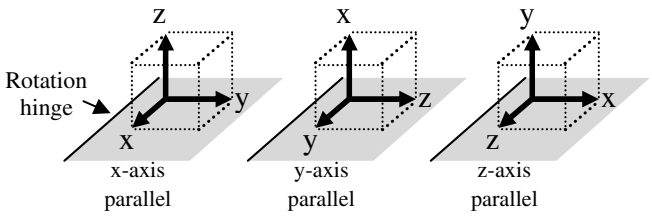

Figure 3. Three cases of the IMU with one axis parallel to the rotation hinge (dark edge of the gray surface) for gyroscope calibration.

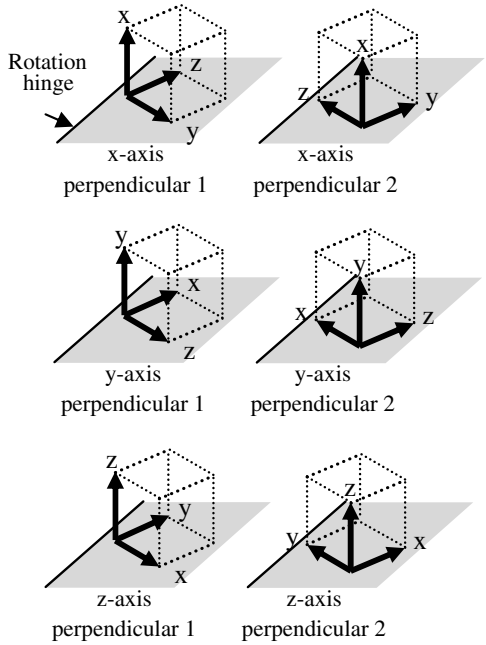

Figure 4. Six cases of the IMU with one axis perpendicular to the rotation hinge (dark edge of the gray surface) for gyroscope calibration.

the angular velocities are non-zero. Therefore, the motion prescribed in the following paragraph is meant to ensure that the errors due to each model parameter are accumulated such that the effect in the divergence is significant. If the amount of rotation is small, the accumulated errors will be of smaller values and can be overwhelmed by the effect of the random noise, which in turn can adversely affect the nonlinear optimization process.

The IMU is mounted in nine different positions, where three of the positions have one of the axes parallel to the hinge, as illustrated in figure 3. If the IMU is perfectly mounted, it would measure zero readings about the other two axes. However, perfect mounting is not required in this calibration method as the angular velocities about all three axes are measured simultaneously and the use of property (**p2**) provides the constraint to compute the model parameters. As illustrated in figure 4, each of the remaining six positions has one axis perpendicular to the hinge and the other two axes at an angle of approximately 45°. This gives non-zero measurements about the two axes and better exposes the misalignment and cross-axis sensitivity parameters. The clockwise and counter-clockwise rotations of 180° about the hinge give a total of 18 sets of data. For ease of reference, this procedure is denoted as procedure 2. The process of computing the gyroscope error model parameter values uses the same nonlinear optimization method as in the case of the accelerometers.

4.3. In-field collection of calibration data (procedure 3)

The proposed gyroscope calibration method imposes no restrictions on the type of rotations between the static states. This, together with the fact that accelerometer calibration does not require precise inclinations and the use of the quasi-static detector, enables the IMU to be calibrated using data that are collected less rigorously. This would allow non-technical users to calibrate future commercial units, enabling widespread applications.

The proposed data collection and processing method, hereafter referred to as procedure 3, consists of first keeping the IMU stationary for a period of time, which is determined using the Allan variance, so that the gyroscope biases are effectively removed. For the current IMU, this period is 20 s. The IMU is moved and paused at least 24 times, that is twice the number of accelerometer error model parameters, to obtain the static acceleration measurements and gyroscope readings for calibrating both types of sensors. The quasi-static detector is used to indicate to the user that the IMU has been kept below a pre-defined quasi-static threshold for a preset period of time, after which the IMU can be moved again. In practice, a threshold of $1.16 \times 10^{-4}\ g^2$ and a period of 0.25 s are found to be suitable values for obtaining good calibration data. To provide an additional buffer against bad data points, the IMU is moved and paused a total of 30 times, instead of 24 times. Finally, two variations are considered, the first variation involves the IMU being held in the hand (procedure 3(hand)) and the second with the IMU mounted on a user's head (procedure 3(head)). For procedure 3(hand), the IMU is left stationary for 20 s for the initial gyroscope bias measurement. For procedure 3(head), this stationary period is reduced to 2 s as it is found that it is difficult for a user to keep his head still for 20 s.

The resultant value of the accelerometer cost function, $\boldsymbol{L}(\boldsymbol{\theta}_a)$, in equation (4) provides an indication of the residue error, as well as the quality of the data. The quasi-static threshold is varied from $5.8 \times 10^{-5}\ g^2$ to $3.5 \times 10^{-4}\ g^2$ in steps of $5.8 \times 10^{-5}\ g^2$, and the static time is varied from 0.05 to 0.5 s, in steps of 0.05 s, to find the best values to use for a set of data. The search across a range of quasi-static threshold values and static times is performed because the motion profile is uncontrolled and the residue error is used to find the least noisy set of static gravity vector measurements. The number of quasi-static sets will vary depending on the threshold, the length of static time and the motion profile. Generally, shorter time lengths will give a greater number of quasi-static pauses, which tend to be noisier as well. Contrary to intuition, higher thresholds can result in a lower number of quasi-static stages. This is because there are cases where the IMU is moved very slightly, which would cause the data to be separated into two sections when the threshold is low, and considered to be continuously static when the threshold

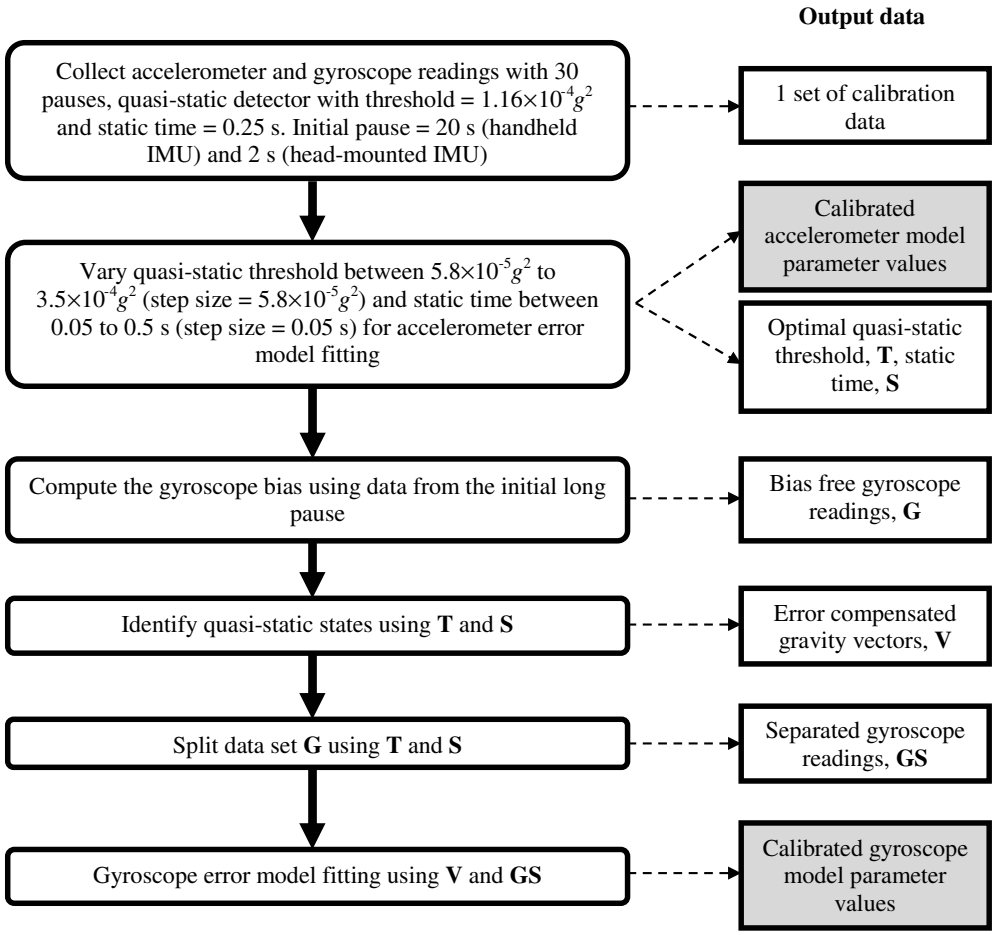

Figure 5. The procedural flow for in-field calibration data collection.

is high. The stated ranges are determined empirically to give good calibration results. When the quasi-static threshold is set below $5.8 \times 10^{-5}\ g^2$, the number of sets obtained is frequently less than 30, as the IMU is subjected to minute vibrations of the hand or head. Furthermore, sets of measurement with the lowest residue error are rarely obtained with quasi-static threshold above $3.5 \times 10^{-4}\ g^2$. Therefore, setting this upper threshold reduces the amount of computation. Setting the step size less than $5.8 \times 10^{-5}\ g^2$ generally produces slight improvement with large increase in computation time. The variance of the accelerometer readings for each of the three axes is used to ensure that the IMU is moved sufficiently. In this case, a minimum variance of 0.2 g for each axis is found to be sufficient to ensure that most motions in the data set are at least 10° apart. If the range of motion is too small, the nonlinear optimization process may not produce meaningful results.

The above process simultaneously determines the values of the accelerometer error model parameters, quasi-static threshold and the length of the static time, which gives the lowest value of the cost function, after which the accelerometer is considered to have been calibrated. Next the gyroscope data are separated into sets using the quasi-static states determined using the optimal threshold and time. The gyroscope biases measured using the initial long pause of the IMU allows the bias to be effectively removed from all the gyroscope readings. The non-random errors in the accelerometer readings are compensated using the accelerometer error model parameter values, to obtain the gravity vectors. The bias-free gyroscope readings and gravity vectors are used to compute the parameter values of the gyroscope error model.

In summary, the data collected using the proposed procedure are first analyzed to obtain the static accelerometer readings for the calibration method presented in section 4.1. The result from the first step is then used to analyze the gyroscope readings to provide the data required by the method presented in section 4.2. Figure 5 illustrates the process graphically.

5. Calibration results and analysis

The results in this section are obtained from the data collected using a custom-built IMU, measuring 51 mm × 35 mm × 12 mm, which forms a part of an AR hybrid tracker. The tri-axial accelerometer and gyroscopic system give rise to a total of six sensor outputs. Each sensor output is sampled at a rate of 1000 Hz, implying that 6000 sensor readings are collected per second. Figure 6 shows a picture of the IMU.

5.1. Accelerometer calibration with controlled data

To study the effects of noise in the measurements, 30 sets of 18 measurements were collected to obtain the mean and the

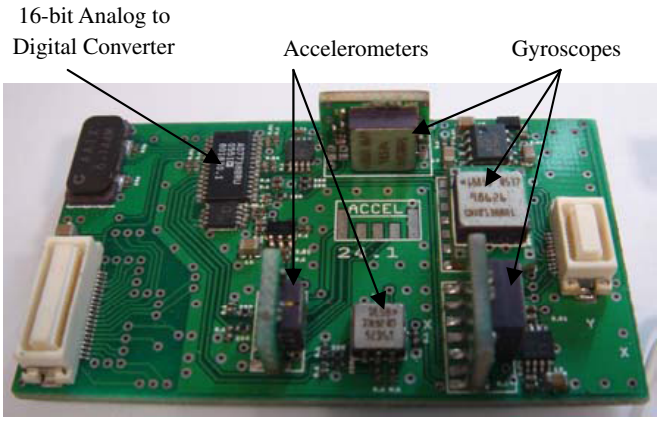

Figure 6. The custom-made inertial measurement unit (IMU) used in the experiments.

(This figure is in colour only in the electronic version)

Table 1. Mean and standard deviation of all the parameter values (dimensionless) obtained from calibration using 30 sets of data. The scale factor and bias parameters are highlighted.

	Mean	Standard deviation
e_{00}	1.001	0.002
e_{01}	0.010	0.008
e_{02}	0.005	0.012
e_{10}	−0.010	0.008
e_{11}	1.009	0.002
e_{12}	0.013	0.011
e_{20}	0.014	0.012
e_{21}	0.015	0.010
e_{22}	1.000	0.002
b_x	0.025	0.002
b_y	−0.022	0.002
b_z	0.019	0.002

standard deviation of the model parameter values, as shown in table 1. The large number of repetitions of procedure 1 and the resultant low standard deviation values provide evidence that proper data for the nonlinear optimization process can be collected using the proposed controlled data collection process.

Each of the 30 sets of data provides a noise contaminated measurement of the model parameters. To make the best use of all the data collected, the mean values in table 1 are used to define the resultant error model for the tri-axial accelerometers in the prototype IMU:

$$\boldsymbol{a}_{P,k} = \begin{pmatrix} 1.001 & 0.01 & 0.005 \\ -0.01 & 1.009 & 0.013 \\ 0.014 & 0.015 & 1.000 \end{pmatrix} \left(\boldsymbol{a}_{S,k} - \begin{pmatrix} 0.025 \\ -0.022 \\ 0.019 \end{pmatrix} \right). \tag{14}$$

To show that the errors are effectively compensated, 100 measurements were taken with the IMU mounted in various positions. The average and maximum magnitudes of the errors from the ideal 1 g are shown in table 2. The average deviation and consequently the errors of the inclination angle are reduced by approximately five times.

Table 2. The average and maximum observed magnitudes of errors from the ideal 1 g, for the measured static accelerations. The angular errors are shown in brackets.

	Average error (mg)	Max observed error (mg)
No calibration	20.1 (1.15°)	44.9 (2.57°)
With calibration	40.0 (0.23°)	28.1 (1.61°)

Table 3. The mean and standard deviations of gyroscope error model parameter values (dimensionless).

	Mean	Standard deviation
e_{00}	0.944	0.006
e_{01}	0.000	0.001
e_{02}	−0.008	0.002
e_{10}	−0.015	0.001
e_{11}	0.947	0.008
e_{12}	−0.008	0.003
e_{20}	−0.015	0.001
e_{21}	0.004	0.004
e_{22}	0.998	0.003

The results in table 2 show that the prototype IMU has an average angular error of 0.23° ($\sin^{-1}(0.0040)$) and a maximum error of 1.61° ($\sin^{-1}(0.0281)$) for either the pitch or roll angles after calibration. As the magnitude of the gravity vector is assumed to be the only quantity known, the angular error here is calculated for the worst case, where the full error appears on a single accelerometer axis which is perfectly horizontal, i.e., perpendicular to the gravity vector. An error of $\sin(\theta)g$ will result in the pitch or roll angle being measured as θ° instead of zero.

5.2. Gyroscope calibration with controlled data

For the gyroscope calibration, procedure 2 was repeated to ascertain its stability in the presence of measurement noise. After four repetitions, the computed values of the gyroscope error model parameter remained consistent and no further repetitions were made. Table 3 shows the mean and standard deviations of each parameter.

As in the case of the accelerometers, to make use of all the data statistically, the mean values are used to define the gyroscope error model for the prototype IMU:

$$\boldsymbol{g}_{P,k} = \begin{pmatrix} 0.944 & 0.000 & -0.008 \\ -0.015 & 0.947 & -0.008 \\ -0.015 & 0.004 & 0.998 \end{pmatrix} (\boldsymbol{g}_{S,k}) \tag{15}$$

To illustrate that the model in equation (15) effectively compensates the gyroscope errors, the average magnitude of the error vector between $\boldsymbol{u}_g$ and $\boldsymbol{u}_a$ is computed, with and without applying the model. The original raw data collected for the calibration, denoted as the *calibration set*, are used. In addition, two test sets of raw data are used. The first test set, *test set* 1, consists of 26 samples, of which 18 samples were obtained using the same motion profile described in procedure 2, except that the angle of rotation is 90° instead of 180°. For the remaining eight samples, the IMU is mounted so that none

Table 4. Average magnitude of divergence and angular deviation between $\boldsymbol{u}_g$ and $\boldsymbol{u}_a$, with and without applying the gyroscope error model in equation (15).

	Calibration set (mg)	Test set 1 (mg)	Test set 2 (mg)
Without gyroscope error model	213.7 (12.30°)	342.0 (19.70°)	236.7 (13.60°)
With gyroscope error model	37.5 (2.15°)	65.4 (3.75°)	098.1 (5.62°)

Table 5. The mean and standard deviations of the accelerometer error model parameter values (dimensionless).

	Procedure 1		Procedure 3 (hand)		Procedure 3 (Head)	
Parameters	Mean	Standard deviation	Mean	Standard deviation	Mean	Standard deviation
e_{00}	1.001	0.002	1.000	0.002	0.997	0.005
e_{01}	0.010	0.005	0.003	0.012	−0.017	0.025
e_{02}	0.005	0.012	0.004	0.011	0.017	0.024
e_{10}	−0.010	0.008	−0.006	0.010	0.014	0.024
e_{11}	1.009	0.002	1.008	0.002	1.004	0.014
e_{12}	0.013	0.011	0.007	0.016	0.015	0.011
e_{20}	0.014	0.012	0.013	0.010	0.002	0.024
e_{21}	0.015	0.010	0.022	0.014	0.010	0.010
e_{22}	1.000	0.002	0.999	0.001	0.996	0.006
b_x	0.025	0.002	0.024	0.001	0.026	0.008
b_y	−0.022	0.002	−0.022	0.001	−0.017	0.015
b_z	0.019	0.002	0.019	0.001	0.021	0.006

of the axes is parallel to the rotation axis. A rotation of 90° in one direction about the rotation axis causes the gyroscopes on all three axes to measure non-zero angular velocities. As there are two possible directions of rotation per axis, this gives rise to the remaining eight possible combinations. The second test set, *test set* 2, consists of 30 samples which are divided into six groups. Each group consists of five samples where the motion is a simple rotation of 180° in a single direction, about one axis of the IMU. As there are three axes and two directions of rotation, there is a total of six rotations. A further variation for *test set* 2 is that the data were collected at an ambient room temperature which is approximately 10 °C higher. As variation due to the temperature is not the focus of this study, accurate temperatures are not measured. All three data sets have 20 s of static data to determine the gyroscope bias.

By validating the gyroscope error model against *test set* 1 and *test set* 2, which are not collected using procedure 2, it can be shown that the effectiveness of the model in equation (15) is not limited to the prescribed motions used during calibration, but applies for general cases as well. Table 4 shows the results and the angular deviation is determined by forming an isosceles triangle with vectors $\boldsymbol{u}_g$ and $\boldsymbol{u}_a$ as the two equal sides and vector $(\boldsymbol{u}_g - \boldsymbol{u}_a)$ as the base. When the IMU is in motion, the dynamic orientation is maintained using only the gyroscopes as the accelerometer measures accelerations in addition to gravity. Without applying the sensor error model, the divergence of $\boldsymbol{u}_g$ and $\boldsymbol{u}_a$ can cause an angular error greater than 10° for all three sets of data, as shown in table 4, which is visually perceptible. The error is reduced five times after applying the model in equation (15) for the *calibration* set and the *test set* 1, making the error less perceptible. As correction is not effective during motion, a lower divergence allows the dynamic orientation to be accurate over a longer period of time. For *test set* 2, the parameter values have changed due to temperature changes, as pointed out by El-Diasty *et al* (2007). However, the error is still reduced more than two times.

5.3. Calibration with data collected using handheld and head-mounted IMU

Experimental results presented in sections 5.1 and 5.2 demonstrate that both the accelerometer and gyroscope model fitting procedures are able to perform consistently with the data collected in pre-determined manners. In this section, the already imprecise motion profiles for procedures 1 and 2 are disregarded. As the cost functions for both sensors do not require known motion profiles, the main purpose now is to demonstrate that the nonlinear model fitting process can work with data of arguably lower quality. As in section 5.2, procedure 3 is repeated to ascertain its stability, and because the data are expectedly noisier, ten repetitions are made. Tables 5 and 6 show the mean and standard deviations of the error model parameter values for the accelerometer and the gyroscope, respectively. The values are computed using the controlled data collection; handheld IMU and head-mounted IMU are placed together for ease of comparison.

From table 5, the results for procedure 3(hand) and procedure 1 agree well. A standard statistical hypothesis test, which is the two sample *t*-test, is used to determine the presence of any significant difference through examining the two-tail *P*-values. From the test, it is found that only e_{01} and e_{21} have *P*-values less than 0.1, which indicates the presence of significant statistical difference. Ten out of twelve parameters are not statistically different; this can be attributed to the fact that both procedures are performed with the IMU held in the hand. The controlled method has specific positions for placing the IMU and a longer static time. The less rigorous method compensates for the random placements of the IMU through using more static samples, checking that the IMU is moved sufficiently as well as searching for the best quasi-static threshold and static time to use. For procedure 3(head), the *P*-values for the two sample *t*-test for eight out of twelve parameters are less than 0.1, indicating that this procedure may

Table 6. The mean and standard deviations of the gyroscope error model parameter values (dimensionless).

	Procedure 2		Procedure 3 (hand)		Procedure 3 (head)	
Parameters	Mean	Standard deviation	Mean	Standard deviation	Mean	Standard deviation
e_{00}	0.944	0.006	0.949	0.005	0.944	0.006
e_{01}	0.000	0.001	−0.003	0.013	0.014	0.029
e_{02}	−0.008	0.002	−0.004	0.011	0.009	0.028
e_{10}	−0.015	0.001	−0.007	−0.013	−0.022	0.025
e_{11}	0.947	0.006	0.948	0.019	0.945	0.021
e_{12}	−0.008	0.003	−0.034	0.027	−0.032	0.014
e_{20}	−0.015	0.001	−0.014	0.011	−0.028	0.024
e_{21}	0.004	0.004	0.026	0.032	0.033	0.017
e_{22}	0.998	0.003	1.003	0.017	1.001	0.009

Table 7. Comparison of the average and maximum magnitudes of errors for the same accelerometer test data, compensated with model parameters obtained using the three procedures.

	Average error (mg)	Max observed error (mg)
No calibration	20.1 (1.15°)	44.9 (2.57°)
Procedure 1	40.0 (0.23°)	28.1 (1.61°)
Procedure 3(hand)	44.0 (0.25°)	29.4 (1.68°)
Procedure 3(head)	53.0 (0.30°)	30.0 (1.72°)

Table 8. Comparison of the average magnitudes of divergence, angular deviation between $\boldsymbol{u}_g$ and $\boldsymbol{u}_a$ for the same gyroscope test data sets, compensated with model parameters obtained using the three procedures.

Gyroscope	Calibration set (mg)	Test set 1 (mg)	Test set 2 (mg)
No calibration	213.7 (12.30°)	342.0 (19.70°)	236.7 (13.60°)
Procedure 2	37.5 (2.15°)	65.4 (3.75°)	98.1 (5.62°)
Procedure 3(hand)	70.2 (4.02°)	69.0 (3.95°)	107.9 (6.19°)
Procedure 3(head)	83.0 (4.76°)	73.2 (4.19°)	108.2 (6.20°)

not perform well. This is mainly because the range of motion is restricted and this lack of variability is manifested in the increased standard deviations of the parameter values. This is frequently the case for nonlinear optimization where the effect of noise is more significant when the spread of the input data is low.

To further elucidate the difference in the performance of the three procedures, the raw data used to obtain the results in table 2 are reused. Table 7 shows the average magnitude of the error and the maximum observed error from 1 *g*, with error compensation using parameter values obtained from each of the three procedures. The results show that the average errors are reduced by at least a factor of 3 and the difference in the performance among the three procedures is small relative to overall error reduction. Although there is degradation in the performance when the random motions are used, the results show that the additional data processing described in section 4.3 mitigates the detrimental effects well.

For the gyroscopes, the results in table 6 show that the parameter values for procedure 3(hand) and procedure 3(head) have larger standard deviations. This is expected due to the randomness of the motion profile. For the case of procedure 3(head), the large standard deviations can also be attributed to the restricted range of motion and the shorter initial static time for measuring the gyroscope biases. The results from the two sample *t*-tests are inconclusive as for procedure 3, only one parameter shows significant statistical difference from procedure 2. As with the accelerometers, the raw data used to obtain the results in table 4 are reused to study the performance of the three procedures. The results are shown in table 8. The parameter values obtained using all three procedures reduce the systematic gyroscope errors to similar levels for each data set. The only exception is when procedure 2 is tested with the calibration set, where the parameter values have been specifically fitted to the data and the angular error is reduced by a factor of 5.7. The reduction factors for procedure 3(hand) and procedure 3(head) are 3.1 and 2.6 respectively for the calibration set. For test sets 1 and 2, all three procedures have similar reduction factors of 5 and 2 respectively. Therefore, it is evident that both procedure 3(hand) and procedure 3(head) have similar performance as procedure 2 despite having larger standard deviations. One possible reason is that the scale factor error is the dominant gyroscope error in this case and the values obtained using all three procedures are similar. For the custom IMU, all three procedures can be used for effective gyroscope calibration.

In the final analysis, while the cost function derived in this research has eliminated the requirement for comparison with precise external inclinations and turn rates, there is still the need to provide low noise data that are well distributed over the range of inputs. This is well illustrated by the increased variability of the computed parameter values as the quality of the data is degraded. In the case of the accelerometer calibration, procedure 1 does not require significantly more effort than procedure 3. Therefore, the final accelerometer calibration technique is to provide a list of positions to place the IMU, as in procedure 1, and apply the data processing steps in procedure 3, to capitalize on the best features of both techniques. In contrast, procedure 2 for the gyroscope is more laborious, as it requires remounting the IMU and longer data collection times, often taking more than an hour to perform all 18 rotations. For procedure 3, there is no additional effort for gyroscope calibration as all the data are collected while calibrating the accelerometer, and each set of data only requires a few minutes to collect.

The above results and analysis show that if sufficient repetitions of procedure 3(hand) are made, ten in this case,

the performance in error compensation can approach that of the controlled procedures 1 and 2. This result is significant for casual users as it means that IMU can be calibrated by simply moving the IMU held in the hands.

6. Conclusion and future works

The proposed error models and calibration methods are able to compensate sensor error and thereby improve the accuracy of the readout of low cost sensors, without any comparison to generated truth values. Applying procedure 1 to the accelerometers in the prototype IMU, the average observed pitch or roll angle error is 0.23°, which represents a reduction ratio of 5 as compared to the errors without calibration. The observed maximum error is also reduced by a factor of 1.6 to 1.61°. Using procedure 2, there is a minimum reduction factor of 2, for the dynamic angular divergence due to the gyroscope sensor errors. These methods are accessible to IMU developers who do not have specialized calibration equipment. With low-cost IMUs, it may not be cost effective to acquire specialized calibration equipment. Furthermore, with a low sensor signal-to-noise ratio, traditional calibration techniques may not provide significant improvements. As the current IMU is mainly used as an orientation sensor in a hybrid AR tracker, an accuracy of 0.23° is adequate for maintaining the illusion of proper augmentation. Procedure 3, which can handle random motions, enables IMUs to be easily calibrated by casual users so as to reduce the average static error to 0.30° and reduce the dynamic angular divergence by more than a factor of 2, when at least ten repetitions are made. This level of ease of inertial sensors calibration has not been achieved in previous methods. Instead of trying to accurately generate the accelerations and angular velocities to directly calibrate the inertial sensors, related properties that are simpler to generate are used. In this case, it is the use of the easily available gravity vector and the constraints imposed by the orthogonal sensor layout that enable the use of more complicated computations to reduce the need for accurate motions and physical mountings.

As the methods are based on gravity and mathematical reasoning, the confidence in them can be further increased by comparing the results against generated truth values. Unfortunately, certified equipment is not available. However, it is precisely because the IMU can be calibrated without external equipment, which allows for the simple-in-field calibration methods proposed here. It is also possible to automate the data collection process and calibrate the IMU automatically without user intervention. This has been applied for accelerometers (Lötters *et al* 1998) and is now possible for gyroscopes with the methods proposed here. This can reduce the production time and cost during mass production as the IMU can calibrate itself during use. Procedure 3 is a step in the direction toward self-calibrating IMUs. The sensor data can be collected while the IMU is in normal use and analyzed in a fashion similar to procedure 3 to extract sets of data for calibration purposes. As the optimization process is relatively slow, the data can be stored for later analysis that is done offline. Although it is not possible to make these low cost sensors into navigation grade instruments, they can be easily made into accurate orientation sensors and short-term positional trackers as part of hybrid systems.

References

Analog 2006 Datasheet for ADXL103/203 accelerometer. Available at http://www.analog.com/UploadedFiles/Data_Sheets/ADXL103_203.pdf (Last Accessed: March 2008)

El-Diasty M, El-Rabbany A and Pagiatakis S 2007 Temperature variation effects on stochastic characteristics for low-cost MEMS-based inertial sensor error *Meas. Sci. Technol.* **18** 3321–8

El-Gizawy M, Noureldin A and El-Sheimy N 2006 A reliable modeless mobile multi-sensor integration technique based on RLS-lattice *Meas. Sci. Technol.* **17** 51–61

Foxlin E and Naimark L 2003 Miniaturization, calibration and accuracy evaluation of a hybrid self-tracker *Proc. 2nd IEEE/ACM ISMAR (Tokyo, 7–10 October 2003)* pp 151–60

Grewal M, Henderson V and Miyasako R 1991 Application of Kalman filtering to the calibration and alignment of inertial navigation systems *IEEE Trans. Autom. Control* **36** 4–13

Jekeli C 2000 *Inertial Navigation Systems with Geodetic Applications* (Berlin: de Gruyter)

Kim A and Golnaraghi M 2004 Initial calibration of an inertial measurement unit using an optical position tracking system *Proc. IEEE PLANS (Monterey, 26–29 April 2004)* pp 96–101

Lötters J C, Schipper J, Veltink P H, Olthuis W and Bergveld P 1998 Procedure for in-use calibration of triaxial accelerometers in medical application *Sensors Actuators* A **68** 221–8

Niu X and El-Sheimy N 2005 Development of a low-cost MEMS IMU/GPS navigation system for land vehicles using auxiliary velocity updates in the body frame *Proc. ION GNSS (California, 13–16 Sep 2005)* pp 2003–12

Press W, Flannery B, Teukolsky S and Vetterling W 1992 *Numerical Recipes in C: The Art of Scientific Computing* (Cambridge: Cambridge University Press)

Sabatini A 2006 A wavelet-based bootstrap method applied to inertial sensor stochastic error modelling using the Allan variance *Meas. Sci. Technol.* **17** 2980–8

Savage P 1998 Strapdown inertial navigation integration algorithm design part 1: attitude algorithms *J. Guid. Control Dyn.* **21** 19–28

Saxena A, Gupta G, Gerasimov V and Ourselin S 2005 In use parameter estimation of inertial sensors by detecting multilevel quasi-static state *Lect. Notes Comput. Sci.* **3684** 595–601

Semeniuk L and Noureldin A 2006 Bridging GPS outages using neural network estimates of INS position and velocity errors *Meas. Sci. Technol.* **17** 2783–98

Skog I and Händel P 2006 Calibration of a MEMS inertial measurement unit *Proc. 17th IMEKO World Congress (Rio de Janeiro, 17–22 September 2006)*

Syed Z F, Aggarwal P, Goodall C, Niu X and El-Sheimy N 2007 A new multi-position calibration method for MEMS inertial navigation systems *Meas. Sci. Technol.* **18** 1897–907

Titterton D and Weston J 1997 *Strapdown Inertial Navigation Technology* (London: Peter Peregrinus) (on behalf of Institution of Electrical Engineers)